

See discussions, stats, and author profiles for this publication at: <https://www.researchgate.net/publication/310048683>

Hot electron engineering for boosting electroluminescence efficiencies of silicon-rich nitride light emitting...

Article · November 2016

DOI: 10.1016/j.jlumin.2016.11.020

CITATIONS

0

READS

35

6 authors, including:



Yonder Berencén

Helmholtz-Zentrum Dresden-Rossendorf

57 PUBLICATIONS 259 CITATIONS

[SEE PROFILE](#)



José Antonio Rodríguez

University of Havana

45 PUBLICATIONS 467 CITATIONS

[SEE PROFILE](#)



Carlos Domínguez

Spanish National Research Council

256 PUBLICATIONS 2,520 CITATIONS

[SEE PROFILE](#)



Blas Garrido

University of Barcelona

275 PUBLICATIONS 3,241 CITATIONS

[SEE PROFILE](#)

Some of the authors of this publication are also working on these related projects:



pHotonics ELelectronics functional Integration on CMOS [View project](#)



Light emitting and electro-optical integrated devices in silicon photonics CMOS technology. Towards disruptive and smart silicon solid state lighting and functional optical interconnects (LEOMIS) [View project](#)



Hot electron engineering for boosting electroluminescence efficiencies of silicon-rich nitride light emitting devices

Y. Berencén^{a,1,*}, B. Mundet^{a,2}, J.A. Rodríguez^{b,3}, J. Montserrat^c, C. Domínguez^c, B. Garrido^a

^a MIND-IN2UB, Departament d'Electrònica, Facultat de Física, Universitat de Barcelona, Martí i Franquès 1, 08028 Barcelona, Spain

^b Instituto Superior Politécnico de Tecnologías e Ciências (ISPTEC), Av. Luanda Sul, Rua Lateral Via S10, Talatona, Belas, Luanda, Angola

^c Instituto de Microelectrónica de Barcelona (IMB-CNM,CSIC), Campus Universidad Autónoma de Barcelona, Bellaterra 08193, Barcelona, Spain

ARTICLE INFO

Article history:

Received 22 September 2016

Received in revised form

4 November 2016

Accepted 5 November 2016

Available online 12 November 2016

Keywords:

Hot electron engineering

Silicon-rich nitride

Electrical transport

Electroluminescent devices

ABSTRACT

The combination of a SiO₂ electron accelerator layer with a silicon-rich nitride layer forming a bilayer embedded in a metal-oxide-semiconductor structure has proved to enhance the integrated visible-infrared EL intensity by more than two orders of magnitude in comparison to the single-layer electroluminescent device approach. The origin of such an improvement is attributed to the massive ionization of defects in the silicon-rich nitride layer by direct impact of injected hot electrons coming from the SiO₂ conduction band. Our premises are further corroborated by performing a thorough study of the charge transport in the bilayer structure. This study displays a main electrical mechanism at steady state that combines hot-electron tunneling injection from the SiO₂ accelerator layer and space charge-limited current enhanced by Poole-Frenkel conduction from the silicon-rich nitride electroluminescent layer. The proposed electrical mechanism is validated by numerical simulations that provide good agreement with the experimental behavior. These results point out the feasibility of boosting electroluminescence efficiency of Si-based light emitting devices by performing an adequate gate stack engineering that maximizes the hot-electron injection into the electroluminescent layer.

© 2016 Elsevier B.V. All rights reserved.

1. Introduction

The development of an efficient integrated Si-based light source through a complementary-metal-oxide-semiconductor (CMOS) compatible technological process would enable the monolithic integration of the photonic functions and the electronic drivers in a Si chip, hence paving the way towards the creation of an electrically driven photonic integrated circuit. This old dream of the scientific community became to be considered a real possibility after the pioneering works of Canham in the early nineties about photoluminescence from porous silicon [1]. Since then, countless challenges have been faced which have spanned from the fabrication and optimization of several Si-based luminescent materials and devices [2–13] to more recent attempts of fabricating building blocks that integrate electrically driven light emitters

into a Si photonic chip [14,15].

Despite significant progress achieved over recent years [4–15], Si-based light emitting devices (LEDs) so far developed do not compete with its III-V or organic compound-based counterparts. One of the most pressing issues that hinders practical applications of these devices is the low electroluminescence (EL) power efficiencies which do not surpass the required threshold. The use of multilayered structures based on Si compound insulating layers (viz. silicon oxides and silicon nitrides) has been one of the most popular approaches to overcome such a hindrance. In particular, special interest has aroused the use of these structures with embedded silicon nanocrystals (Si-ncs) to obtain superior optoelectronic performance, taking advantage of the enhanced current injection and transport provided by a highly ordered Si-nc array [3]. Moreover, the role of SiO₂ as an electron accelerator layer, and especially its ability to control the electron energy when varying the layer thickness has been mentioned in previous works [16–18].

As a proof of concept, we proposed a bilayer design that combines a Tb-doped silicon-rich nitride electroluminescent layer with a SiO₂ layer, obtaining significant external quantum efficiency and green-yellow light emission enhancement from electrically driven MOS devices [19]. In addition, we recently reported on the enhancement of two orders of magnitude of the 1.54-μm EL power efficiency for trivalent erbium (Er³⁺) ions in a Er:Si-nc/Si₃N₄/SiO₂

* Corresponding author.

E-mail address: y.berencen@hzdr.de (Y. Berencén).

¹ Present address: Institute of Ion Beam Physics and Materials Research, Helmholtz-Zentrum Dresden-Rossendorf, 01314 Dresden, Germany.

² Present address: Institut de Ciència de Materials de Barcelona, ICMAB—CSIC, Campus UA Barcelona, Bellaterra, 08193, Barcelona, Spain

³ Permanent address: Facultad de Física-IMRE, Universidad de La Habana, San Lázaro y L, 10400, Plaza, La Habana, Cuba.

bilayer structure [17], where direct impact by hot electrons accelerated by the SiO₂ layer was found to be the fundamental excitation mechanism. The reason for using silicon nitride as a host material to allocate luminescent species in the previous works relies on the fact that it is a mechanically and thermally stable material while it allows for better current injection and transport due to its lower band gap in respect of silicon oxide. Furthermore, silicon nitride has higher robustness, from the electrical standpoint, than silicon oxide because the trapped charge can be easily released via thermally activated shallow trap levels.

Following the precedent working line, in the present work, Si-nc/Si₃N₄/SiO₂ bilayer structure-based light emitting devices with different gate stacks are proposed. A significant enhancement of more than two orders of magnitude for the integrated visible-infrared (IR) EL intensity is reported. Electrical and electroluminescence measurements together with dynamical-transport simulations allowed identifying the main excitation mechanism responsible for this enhancement. The possibility of boosting the hot electron-triggered EL efficiencies by gate-stack engineering for these devices is established.

2. Experimental details

Different devices were fabricated attending to the gate stacking layer. Namely, two SiN_x/SiO₂ bilayer structures and a single (sub-stoichiometric) SiN_x layer as a reference sample. The sample features are listed on Table 1. The SiO₂ layers were fabricated following a thermal dry oxide process over highly *n*-type doped < 100 > Si substrates. The silicon nitride films were obtained in a low-pressure chemical vapor deposition (LPCVD) furnace working at 800 °C and using as precursors dichlorosilane and ammonia with a flow rate of 30/200 sccm and a total pressure of 130 mTorr. The deposition rate was around 3.8 ± 0.3 nm/min. Subsequently, the matrix stoichiometry was modified by introducing 12% of Si excess by means of ion implantation, using a Si dose of around 5.5×10^{16} cm⁻² with an implantation energy of 35 keV. A post-annealing process at 950 °C was performed during 1 hour to recover the dielectric matrix from implantation related-defects and to simultaneously induce the formation of Si-ncs. The gate electrode consists of a semitransparent polycrystalline silicon (PolySi) film of 100 nm-thick, which was deposited by LPCVD at 630 °C and highly-doped *n*-type with phosphoryl chloride (POCl₃) at 900 °C for 20 minutes. A 500 nm-thick aluminum film, annealed at 450 °C in forming gas, was used as back ohmic contact to the Si substrate. Different device areas ranging from 4×10^{-6} cm² to 1.2×10^{-4} cm² were defined and fabricated by conventional optical lithography.

Quasi-static electrical measurements were carried out by a semiconductor device analyzer (Agilent B1500) and a probe station (Cascade Microtech Summit 11000) with a Faraday cage isolation. EL spectra measurements were performed with a cryogenically cooled Princeton Instruments Spec-10-100B/LN charge-coupled device, coupled to an Acton 2300i grating spectrometer. Time-resolved EL experiments were conducted in order to determine the lifetimes of the luminescent species. EL decay traces were recorded using a digital GHz oscilloscope linked to a

Table 1
Devices under study.

Device	Layer material and thickness	
	SiO ₂ (thermal)	SiN _x (LPCVD)
SiO25/SiN20	25 nm	20 nm
SiO10/SiN30	10 nm	30 nm
SiN30	–	30 nm

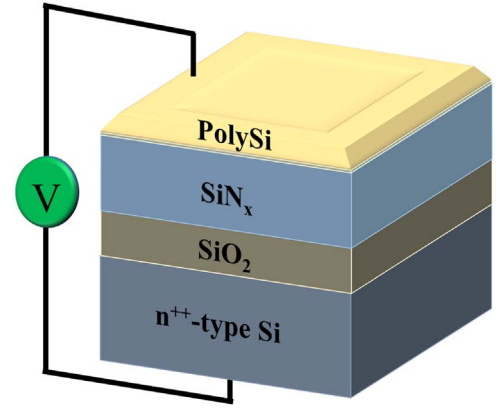


Fig. 1. Sketch of the device cross section and bias schema.

photomultiplier tube (R928) synchronously triggered by an Agilent 8114 A pulse generator. All electrical and EL measurements were driven at room temperature with a positively biased gate electrode. This means that electrons coming from Si substrate are forced to enter into the SiN_x layer through the SiO₂ one. All measured spectra were corrected with the optical response of the system. A cross sectional view of the studied devices is sketched on Fig. 1.

3. Results and discussion

3.1. Electrical properties

Fig. 2(a) shows the electrical characteristics for all samples as well as their corresponding simulated I-V curves, obtained according to the simulations described in the Appendix. It is clearly observed that the device conductivity decreases as the thickness of the SiO₂ layer increases, being SiO25/SiN20 the device gate stack with the lowest conductivity followed by SiO10/SiN30 and SiN30 layer, respectively. Moreover, the three samples show a similar I-V trend, suggesting a common transport mechanism. Interestingly, the SiO₂ layer introduces a flat region at low voltages that is not observed in the reference sample (SiN30). This region has commonly been associated to the displacement currents due to capacitance effects [19], and denotes larger capacitance in samples with SiO₂ layer. Being the capacitance equal to the ratio of the charge and the applied voltage, we speculate about a larger charge trapping occurring in the bilayer structures (viz. SiO25/SiN20 and SiO10/SiN30) than that of the reference sample (SiN30).

Fig. 2(b) depicts the experimental I-V curves and the data fitting using a combination of two conduction models. This combination is usually referred to as space charge-limited current enhanced by Poole-Frenkel effect (SCLC+PF) and was initially proposed by Murgatroyd [20]. In such a mechanism, the current density (J_{mur}) depends on the voltage and temperature as follows:

$$J_{mur} = \frac{9}{8} \mu \epsilon_r \epsilon_0 \frac{V^2}{L^3} \theta_0 \exp \left[\frac{0.891}{k_B T} \left(\frac{q^3 V}{\pi \epsilon_r \epsilon_0} \right)^{1/2} \right] \quad (1)$$

with

$$\frac{\rho_f}{\rho_f + \rho_t} = \theta_0 = \frac{N_c}{N_t} \exp \left(\frac{E_A}{k_B T} \right),$$

where ρ_f and ρ_t are the free and trapped charge density respectively, N_c is the amount of carriers in the conduction band, ϵ_r is the relative permittivity, μ is the electron mobility, L is the layer thickness, E_A is the activation energy (i.e. the minimum energy

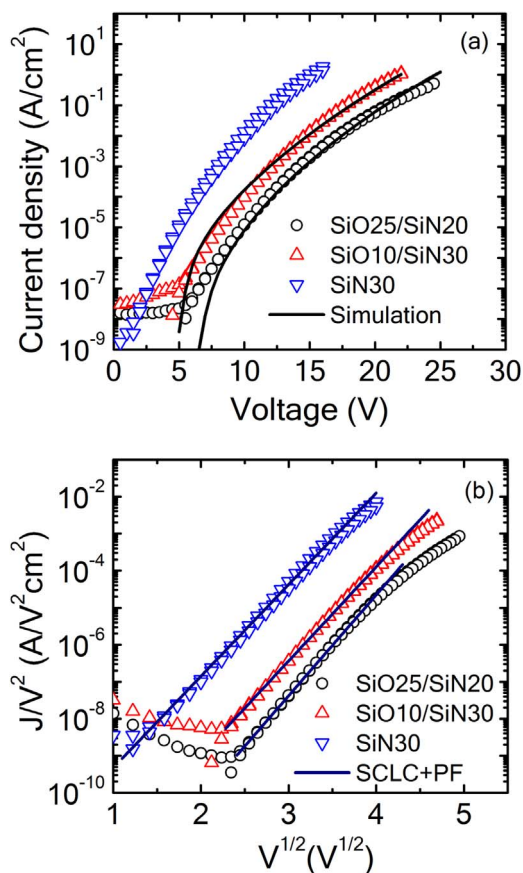


Fig. 2. (a) Experimental electrical characteristics of the studied devices and the corresponding electrical simulations (black solid lines). (b) Poole-Frenkel representation showing the linear fitting to the SCLC + PF mechanism (navy blue solid lines). (For interpretation of the references to color in this figure legend, the reader is referred to the web version of this article.)

required by carriers to surmount the potential barrier height of traps) and k_B , T and ϵ_0 have their usual meanings. From Fig. 2(b) is also observed that the correlation between the experimental and the fitted data is especially good in the whole range of voltages for the reference device (SiN30). On the contrary, at high voltages the fitted model slightly deviates from the experimental curves for the SiO25/SiN20 and SiO10/SiN30 devices.

One criterion commonly used to evaluate the suitability of any applied conduction model is the analysis of the extracted physical parameters. For instance, the relative permittivity of layers can be extracted from the slope of the PF representation shown in the Fig. 2(b). The estimated value for the SiN30 reference device was found to be around 7, which is in good concordance with the one reported for stoichiometric silicon nitride ($\epsilon_r = 7.5$) [21]. Thus, assuming a relative permittivity of around 4 for the SiO₂, it seems reasonable to expect a value that lies between 4 and 7.5 for the bilayers. This is not the case however for the SiO25/SiN20 and SiO10/SiN30 devices. The respective estimated ϵ_r values were a factor of 1.6 and 1.4 higher than that of the physically expected ones. This latter fact suggests a more complex transport mechanism to describe the electrical behaviour for the whole voltage range. Indeed, bearing in mind that SCLC + PF mechanism wholly describes the electrical conduction in the silicon-rich nitride layer [12], we only have to concern about the electrical mechanism occurring in the silicon dioxide. From literature, there is a great number of works that account for this issue, most of them displaying a tunnelling injection in the SiO₂, modelled by either Fowler-Nordheim tunnelling or trap-assisted tunnelling, depending on the layer thickness [22–24]. Therefore, we sequentially

combine two different mechanisms to model the total current arising from *injection* and *transport* mechanisms in our structures. At first, an electrode-limited *injection* mechanism dominated by the barrier height between the PolySi electrode and the SiO₂ layer, and subsequently a bulk-limited *transport* when injected carriers reach the SiO₂/SiNₓ interface. For doing so, we have adapted the model proposed by Arnett [25], which involves numerical calculations. This model has widely been used to understand the electrical properties in random access memories (RAM) [26,27]. The gate stack in both RAM and our devices is completely analogous, which makes the model perfectly applicable to our study. The most important difference between both cases, in terms of gate stack, relies on the SiO₂ thickness (viz. much thicker layers in our case), which might modify the type of tunnelling process that occurs in the SiO₂ layer (viz. direct band-to-band tunnelling or trap-assisted tunnelling). A description of the adapted model is presented in the Appendix.

The results from the electrical conduction simulations are summarized in Fig. 2(a). In particular, Fig. 2(a) indicates the good agreement, in the whole range of voltages, between the simulated I-V curves (black solid lines) and the experimental data for the SiO25/SiN20 and SiO10/SiN30 bilayer devices. This figure also allows extracting conclusive information about the charge *injection* and *transport* in the bilayer structure. In detail, applying a positive voltage to the PolySi gate, electrons coming from the Si substrate are injected into the bilayer following a tunnelling process through SiO₂ layer. This involves a tunnelling *injection* mechanism either by Fowler-Nordheim tunnelling (J_{FN}) or trap-assisted tunnelling (J_{TAT}) depending on the SiO₂ thickness. At the initial stage of carrier injection, most of the intra-band defects in the SiNₓ layer are available and thus electron injection is solely limited by the barrier height between the PolySi gate and the SiO₂ layer (see the band diagram in Fig. 3(a)). From this point on, the intra-band defects start to be gradually filled until the quasi-stationary regime is reached (viz. when trapping rate equals detrapping rate). Then, at such a quasi-stationary regime, the SCLC + PF conduction mechanism begins to dominate over the tunnelling injection process and hence the layer conductivity is mostly governed by the trapping/detrapping rate in the SiNₓ (see Fig. 3(b)).

3.2. Electroluminescence properties

Fig. 4(a) shows the typical EL spectrum for SiO25/SiN20 and its evolution at different current intensity values. The emission spans from 500 nm to 900 nm, with the maximum peaking at 690 nm. In addition, the spectral line-shape does not vary as a function of the injected current, which suggests that all luminescent species are being simultaneously excited from the EL onset. Furthermore, both SiO10/SiN30 and SiN30 reference sample show a very similar spectral behavior and peak position. This fact suggests that the role of the SiO₂ layer on the spectral behavior is rather precluded. The origin of the emission band at 690 nm is thought to be defect-related and further enhanced by the Si excess into the already defective Si₃N₄ matrix [12]. PF ionization generates positively-charged shallow-traps which are susceptible of trapping electrons that may recombine with valence band holes producing photons. Time-resolved EL measurements were accomplished to unambiguously confirm the origin of such an emission. Fig. 4(b) depicts the EL decay trace for the SiO25/SiN20 device under electrical excitation carried out by step-like voltage pulse with a period of 10 μs ranging from 0 V to 20 V. The measured EL trace is well-fitted to a single exponential function, resulting in a value of decay time of around 500 ns. Likewise, the decay times for the SiO10/SiN30 and SiN30 devices were found to be in the order of hundreds of nanoseconds. These values corroborate the origin of luminescent species, which are associated to Si-related defects

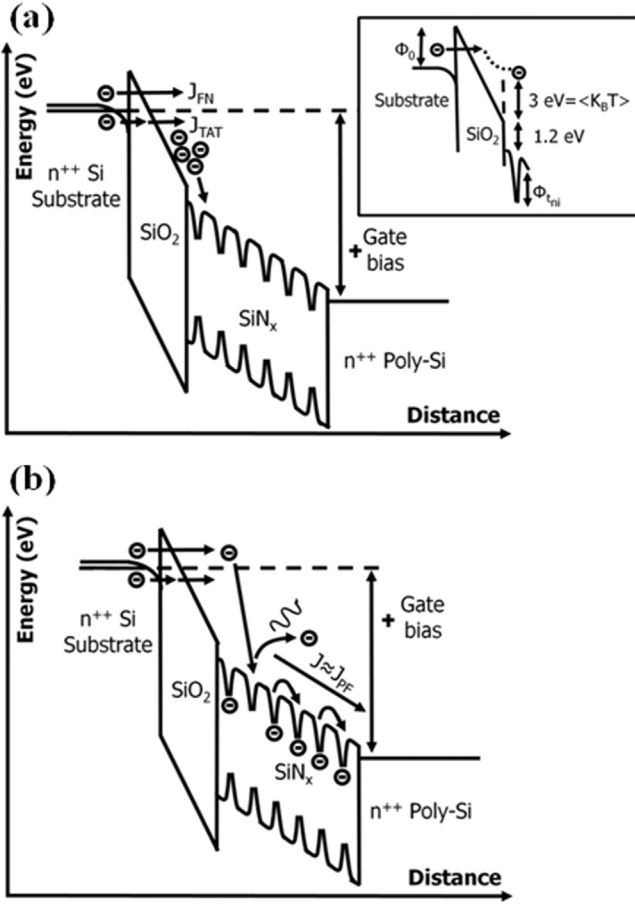


Fig. 3. Sketch of the band diagram and optoelectronic processes under hot electron injection, (a) dynamic regime and (b) quasi-stationary regime. The inset shows the different potential energy barriers for carriers (Φ_0 , Φ_{ni}), the average kinetic energy due to electron-phonon interaction and conduction band-offset at the SiO₂/SiN_x interface.

embedded into the SiN_x material, in accordance with previous published works, where similar electroluminescent layers were studied [10–12].

The integrated EL intensity as a function of the injected current density for all devices is depicted in Fig. 5. A remarkable enhancement of the integrated EL intensity of more than two orders of magnitude is observed when the SiO₂ electron-accelerator layer is incorporated. At a fixed current density of 10⁻¹ A/cm², the SiO₂/SiN₂₀ and SiO₁₀/SiN₃₀ devices exhibit integrated EL intensities which are, respectively, 170 times and 70 times higher than the corresponding to the SiN₃₀ reference device based on a single SiN_x layer.

To understand the electroluminescent mechanism and the significant EL intensity enhancement by incorporating the SiO₂ layer, the knowledge of the average kinetic energy of injected electrons in the bilayer structure is essential. We have recently demonstrated that injected electrons into the SiO₂ conduction band get rapidly accelerated, attaining an average kinetic energy around 3 eV within the very first 10 nm of SiO₂ layer due to the balance between the electric field action and the multiple scattering processes associated to phonons [17]. In addition, an extra energy of around 1.2 eV has to be also taken into account when carriers reach the SiO₂/SiN_x interface due to the difference in electron affinities between SiO₂ and SiN_x. Therefore, electrons finally arrive to the SiN_x conduction band with an average kinetic energy of around 4 eV. Inset of Fig. 3(a) depicts this situation, showing the electron heating process underwent at the SiO₂/SiN_x

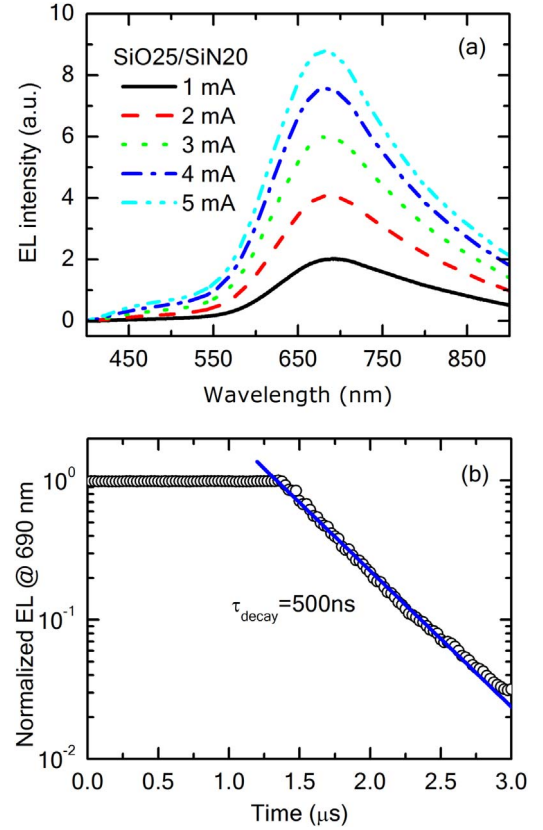


Fig. 4. (a) Recorded EL spectrum for the SiO₂₅/SiN₂₀ device at different driving currents, (b) EL decay trace of the main emission peak at 690 nm, which exhibits a single exponential decay.

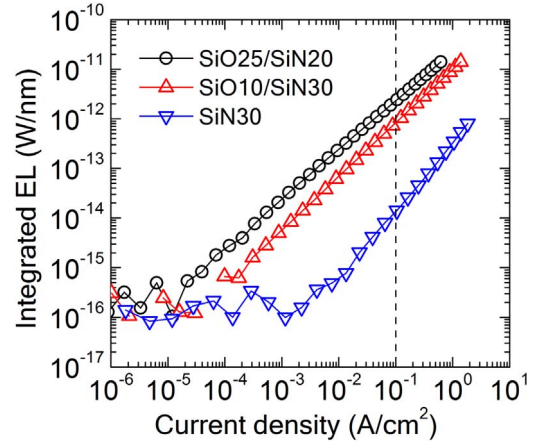


Fig. 5. Integrated EL as a function of the current density for all devices. For the sake of comparison, the collected EL emission is normalized to the thickness of SiN_x active layer for the SiO₂₅/SiN₂₀ and SiO₁₀/SiN₃₀ devices.

interface. Once at the SiN_x conduction band, hot electrons are expected to rapidly cool down after few nanometers due to the large number of non-elastic scattering events as well as the high trapping/detrapping rate [17]. Most of hot electrons in the silicon nitride conduction band can move very short distances before they get trapped by intra-band defects. Moreover, hot electrons at SiN_x are expected to impact and ionize several traps by multiple scattering events in the way down to the bottom of the conduction band. A somewhat similar behaviour was observed in Ref. [18] where the amount of ionized traps in a single Si₃N₄ layer was demonstrated to be strongly reduced due to the low hot-electron generation at the silicon nitride layer itself.

These results point out that i) both the average kinetic energy and the number of hot electrons can be readily enhanced by increasing the SiO₂ layer thickness, but it is worth noticing that there is a limit for further EL enhancement at a distance of 20 nm in SiO₂ (at 7 MeV/cm). We have recently demonstrated that the average electron-kinetic energy becomes constant at this distance [17]. This suggests that 20-nm-SiO₂ thick layers should render the highest EL performance. For thicker SiO₂ layers the gained electron-kinetic energy from the electric field is stabilized by acoustic, polar and non-polar electron-phonon scattering losses [17] and ii) the EL intensity is significantly increased thanks to the combination of two electroluminescent excitation processes, which simultaneously occur at SiN_x viz. PF emission due to defect or trap ionization followed by electron-hole recombination and direct impact excitation by hot electrons coming from SiO₂ conduction band. Therefore, high operating voltages and relatively low density of injected current are required. This fact, however, has consequences for EL efficiency. A promising solution, in the same line of reasoning, might be to pre-heat electrons to high energy in a semiconducting layer at relatively low electric fields prior to injection into the high-field SiO₂ acceleration layer.

4. Conclusions

In summary, the electrical and EL properties from silicon-rich nitride and silicon oxide bilayer-based light emitting devices with different gate stacks to maximize the hot-electron injection were investigated. Numerical simulations were used to unambiguously identify that the carrier *transport* in the investigated devices takes place through a space charge-limited current mechanism enhanced by Poole-Frenkel effect (SCLC+PF), whereas the electron *injection* is either by FN or TAT depending on the SiO₂ layer thickness. For the device with 20 nm-SiN_x and 25 nm-SiO₂ layer thicknesses respectively, a spectrally broad 690-nm EL emission with an integrated intensity two orders of magnitude larger than the corresponding to a single SiN_x layer was obtained. Such an emission was ascribed to the ionization of trapped electrons at the Si-related defects embedded into the SiN_x matrix, according to the lifetime values deduced by time-resolved EL measurements. The ionization of the luminescent centers is achieved through i) impact with hot electrons accelerated at the SiO₂ conduction band under the action of the electric field and ii) by the energy step of 1.2 eV at the SiO₂/SiN_x interface which is produced by the difference in the electronic affinities of both materials. The presented device structure also enables to independently study the mechanisms that give rise to the carrier injection, transport and EL emission processes. This work opens new possibilities of developing efficient Si-based light emitting device via gate stack engineering.

Acknowledgment

The authors acknowledge funding from the Spanish Ministry of Economy and Competitiveness (MINECO) through the project LEOMIS (TEC2012-38540-C02-01). Y.B. acknowledges financial support from the Subprograma de Formación de Personal Investigador FPI-MICINN (TEC2009-08359) and for sample fabrication in the Integrated Nano and Microelectronics Clean Room at IMB-CNM through the ICTS access program (Project ICTS-NGG-260). Y.B. would also like to thank the Alexander-von-Humboldt foundation for providing a postdoctoral fellowship at Helmholtz-Zentrum Dresden-Rossendorf.

Table 2

Used parameters on the simulation.

Parameter	Value
Barrier height at substrate/SiO ₂ interface, ϕ_0	2.8 eV
Trap barrier height in the SiO ₂ , ϕ_{tox}	1.6 eV
Trap barrier height in the SiN _x , ϕ_{tni}	0.7 eV
Relative permittivity of SiO ₂ , ϵ_{ox}	3.9
Electron effective mass in SiO ₂ , m_{ox}^*	0.4 (m_0)
Electron capture cross section, σ	10^{-16} cm ²
Detrapping frequency, ν_0	10^9 s ⁻¹
Doping of Si substrate, N_{subst}	10^{19} cm ⁻³

Appendix

The most important parameters used in the simulation are summarized on Table 2 [18,25].

To apply the proposed model, two main considerations were made: i) the total current in the bilayer structure is governed by the trapping-detrapping dynamic occurring in the available trap states at the band gap of the SiN_x layer and ii) the amount of injected electrons into the SiN_x is only limited by the number of electrons capable of tunnelling from the electrode to the SiO₂ conduction band. Hence, there are two fundamental contributions to the current flowing across the device: i) the one related to the number of carriers connected with the SiN_x traps or defects, and ii) the one associated to the injected hot carriers coming from the SiO₂ conduction band. The first contribution has been modelled considering a bulk-limited conduction in the SiN_x layer and incorporates two terms in the continuity equation (see Eq. (2)). The first term accounts for the trapping rate and the second one accounts for the detrapping rate:

$$\frac{\partial n_t(x, t)}{\partial t} = \frac{J(x, t)}{q} \sigma [N_t - n_t(x, t)] - n_t(x, t) q \nu_0 \exp\left[-(\phi_{tni} - \sqrt{q^3 E_N(x, t) / \pi \epsilon_r \epsilon_0}) / k_B T\right] \quad (2)$$

where N_t and n_t are the amount of available and filled traps in the SiN_x respectively, σ is the trapping cross section, ν_0 is the detrapping frequency, ϕ_{tni} is the energy trap depth (in eV), E_N is the electric field in silicon nitride and J is the current density. Eq. (2) presents the partial derivatives as a function of time and not as a function of coordinates. Therefore, in order to provide the conversion from the temporal to the coordinate space, we firstly calculate the electric field drop in each device layer using both the Poisson (3) and the constitutive Eq. (4):

$$\frac{\partial E_N(x, t)}{\partial x} = \frac{\rho(x, t)}{\epsilon} \quad (3)$$

$$\epsilon_{ox} E_{ox} = \epsilon_{ni} E_{ni} \quad (4)$$

Then, the continuity Eq. (5) is used to correlate the spatial gradient of current density with the temporal derivative of trapped carrier density as follows:

$$\frac{\partial J(x, t)}{\partial x} = - \frac{\partial \rho(x, t)}{\partial t} = - q \frac{\partial [n_c + n_t]}{\partial t} \approx - q \frac{\partial n_t(x, t)}{\partial t} \quad (5)$$

where n_c is the amount of electrons in the conduction band. In a first approximation, we consider that i) $\partial n_c / \partial t < \partial n_t / \partial t$ and ii) the temporal variation of the concentration of electrons located at the conduction band is neglected. Thus, the current density value is calculated at every point of the SiN_x layer by combining Eqs. (2) and (5) and subsequently, we solve the new transport differential equation given by:

$$\frac{\partial J(x, t)}{\partial x} = -J(x, t)\sigma [N_t - n_t(x, t)] + n_t(x, t)q\nu_0 \exp\left[-(\phi_{t_{ni}} - \sqrt{q^3 E_N(x, t)/\pi\epsilon_r\epsilon_0})/k_B T\right] \quad (6)$$

The current density shown in Eq. (5) is calculated by means of Eq. (2) as a function of time and coordinate, taking into account the dynamics of the available trapping sites at the SiN_x layer. Thus, the Eq. (7) is obtained:

$$n_t = \left[\frac{J(x, t)}{q} \sigma [N_t - n_t(x, t)] \right] \times \Delta t - \left\{ n_t(x, t)q\nu_0 \exp\left[-(\phi_{t_{ni}} - \sqrt{q^3 E_N(x, t)/\pi\epsilon_r\epsilon_0})/k_B T\right] \right\} \times \Delta t \quad (7)$$

The number of filled traps (n_t) at any voltage is considered under steady state conditions. In other words, when the trapping and detrapping terms coincide. Hence, the spatial current gradient vanishes and the current becomes constant through the layer, arriving to a quasi-stationary regime. To solve the Eq. (7), the expressions (8) and (9) are used as boundary conditions, according to the following arguments. Indeed, as aforementioned, we take advantage of the fact that all injected electrons in the SiN_x tunnel from the SiO₂ layer. At first instance, the amount of injected carriers in the SiN_x can be calculated using the field-enhanced Fowler-Nordheim (FN) model [22,23]. The commonly used expression for this model is given by:

$$J_{FN} = \frac{q^3}{8\pi h \phi_o} E_{ox}^2 \exp\left(-\frac{8\pi\sqrt{2m_{ox}^*}}{3hqE_{ox}} \phi_o^{3/3}\right) \quad (8)$$

where m_{ox}^* is the effective electron mass in the silicon dioxide, h is the Planck constant, E_{ox} is the electric field in the SiO₂ and ϕ_o is the energetic barrier at the Si substrate and SiO₂ interface. However, for electric fields equal or less than 8 MV/cm and too thick layers, the direct tunneling mechanism from the electrode to the SiO₂ conduction band has low probability of occurrence [23]. In such a case the most probable mechanism is the trap-assisted tunneling (TAT), where SiO₂ intra-band defects or traps assist electrons for the tunneling process. This model essentially follows the same exponential dependency of FN but the potential barrier height at the interface SiO₂/Si substrate (ϕ_o) has to be substituted by the oxide trap depth (ϕ_{tox}) [23,24], accordingly. The TAT relationship holds as follows:

$$J_{TAT} \propto \exp\left(-\frac{8\pi\sqrt{2m_{ox}^*}}{3hqE_{ox}} \phi_{tox}^{3/2}\right) \quad (9)$$

Both expressions give us information about the amount of electrons available at the SiN_x/SiO₂ interface under thermodynamic equilibrium conditions.

References

- [1] L.T. Canham, Appl. Phys. Lett. 57 (1990) 1046.
- [2] J. Warg, R. Li, S.N. Basu, L. Dal Negro, Appl. Phys. Lett. 93 (2008) 151116.
- [3] A. Marconi, A. Anopchenko, M. Wang, G. Pucker, P. Bellutti, L. Pavesi, Appl. Phys. Lett. 94 (2009) 221110.
- [4] Z.H. Cen, T.P. Chen, Z. Liu, Y. Liu, L. Ding, M. Yang, J.I. Wong, S. Yu, W.P. Goh, Opt. Express 18 (2010) 20439.
- [5] M. Perálvarez, J. Carreras, J. Barreto, A. Morales, C. Domínguez, B. Garrido, Appl. Phys. Lett. 92 (2008) 241104.
- [6] D. Li, J. Huang, D. Yang, Physica E 41 (2009) 920.
- [7] A. López-Suárez, J. Fandiño, B.M. Monroy, G. Santana, J.C. Alonso, Physica E 40 (2008) 3141.
- [8] B. Shankar Sahu, F. Delachat, A. Slaoui, M. Carrada, G. Ferblantier, D. Muller, Nanoscale Res. Lett. 6 (2011) 178.
- [9] A.A. González-Fernández, J. Juvert, A. Morales-Sánchez, J. Barreto, M. Acéves-Mijares, C. Domínguez, J. Appl. Phys. 111 (2012) 053109.
- [10] Y. Berencén, J. Carreras, O. Jambois, J.M. Ramírez, J.A. Rodríguez, C. Domínguez, C.E. Hunt, B. Garrido, Opt. Express 19 (2011) A234.
- [11] Y. Berencén, O. Jambois, J.M. Ramírez, J.M. Rebled, S. Estradé, F. Peiró, C. Domínguez, J.A. Rodríguez, B. Garrido, Opt. Lett. 36 (2011) 2617.
- [12] Y. Berencén, J.M. Ramírez, O. Jambois, C. Domínguez, J.A. Rodríguez, B. Garrido, J. Appl. Phys. 112 (2012) 033114.
- [13] O. Jambois, F. Gourbilleau, A.J. Kenyon, J. Montserrat, R. Rizk, B. Garrido, Opt. Express 18 (2010) 2230.
- [14] Hong-Gyu Park, Carl J. Barrelet, Yongning Wu, Bozhi Tian, Fang Qian, Charles M. Lieber, Nat. Photon. 2 (2008) 622.
- [15] J.M. Ramírez, F. Ferrarese-Lupi, Y. Berencén, A. Anopchenko, J.P. Colonna, O. Jambois, J.M. Fedeli, L. Pavesi, N. Prtljaga, P. Rivalin, A. Tengattini, D. Navarro-Urrios, B. Garrido, Nanotechnology 24 (2013) 115202.
- [16] D. Arnold, E. Cartier, D.J. Di Maria, Phys. Rev. B 49 (1994) 10278.
- [17] Y. Berencén, S. Illera, L. Rebohle, J.M. Ramírez, R. Wutzler, A. Cirera, D. Hiller, J. A. Rodríguez, W. Skorupa, B. Garrido, J. Phys. D: Appl. Phys. 49 (2016) 085106.
- [18] D.J. Di Maria, J.R. Abernathy, J. Appl. Phys. 60 (1986) 171727.
- [19] Y. Berencén, R. Wutzler, L. Rebohle, D. Hiller, J.M. Ramírez, J.A. Rodríguez, W. Skorupa, B. Garrido, Appl. Phys. Lett. 103 (2013) 111102.
- [20] P.N. Murgatroyd, J. Phys. D: Appl. Phys. 3 (1970) 151.
- [21] S.M. Sze, Physics of Semiconductor Devices, 2nd ed., Wiley, New York, 1981.
- [22] M. Lenzlinger, E.H. Snow, J. Appl. Phys. 40 (1959) 278.
- [23] M.P. Houn, Y.H. Wang, W.J. Chang, J. Appl. Phys. 86 (1999) 1488.
- [24] S. Fleischer, P.T. Lai, Y.C. Cheng, J. Appl. Phys. 72 (1992) 5711.
- [25] P.C. Arnett, J. Appl. Phys. 46 (1975) 5236.
- [26] F. Martin, X. Aymerich, Microelectron. J. 22 (1991) 5.
- [27] H. Bachhofer, H. Reisinger, E. Bertagnolli, H. von Philipsborn, J. Appl. Phys. 89 (2001) 2791.